SEVENTH EUROPEAN ROTORCRAFT AND POWERED LIFT AIRCRAFT FORUM

Paper No. 5

# AN EXTENSION OF THE LOCAL MOMENTUM THEORY TO THE ROTORS OPERATING IN TWISTED FLOW FIELD

Akira AZUMA, Ken-ichi NASU and Takatoshi HAYASHI

University of Tokyo

September 8 - 11, 1981

Garmisch-Partenkirchen
Federal Republic of Germany

Deutsche Gesellschaft für Luft- und Raumfahrt e. V.

Goethestr. 10, D-5000 Köln 51, F.R.G.

AN EXTENSION OF THE LOCAL MOMENTUM THEORY
TO THE ROTORS OPERATING IN TWISTED FLOW FIELD

By

Akira Azuma, Ken-ichi Nasu and Takatoshi Hayashi
University of Tokyo

## ABSTRACT

The local momentum theory was developed to calculate the dynamic airloading of a helicopter rotor, where the velocity perpendicular to the plane of rotation was assumed to be negligibly low in comparison with the rotating velocity. In the case of propellers or windmills, however, this assumption is no longer adequate, and the flow field seen in the rotor-fixed-coordinate system is noticeably twisted along the span. In order to permit calculation of the induced velocity distribution as well as the airloading of the blade in such a twisted flow field, we have carried out an extension of the local momentum theory. Since our method of calculation is based on the instantaneous circulation distribution rather than the instantaneous momentum balance, it may be called the "Local Circulation Method." The present method is also applicable to propellers and windmills in yawed flow.

## NOMENCLATURE

$a$ , lift slope.
$b$ , number of blades.
$C$ , attenuation coefficient.
$C_d$ , drag coefficient.
$C_\ell$ , lift coefficient.
$C_P$ , power coefficient, $C_P = (\text{power})/\rho\pi R^2(R\Omega)^3$.
$C_T$ , thrust coefficient, $C_T = (\text{thrust})/\rho\pi R^2(R\Omega)^2$.
$C_\Gamma$ , intensity of bound vortex.
$C_{\Gamma k}$, intensity of bound vortex of k-th quasi-elliptic wing.
$c$ , wing chord.
$d$ , section drag.
$\vec{e}$ , unit vector along a stream line.
$H$ , mean value of bound vortex in an interval.
$i$ , angle of rotational plane to the advancing velocity.
$L$ , lift.
$\Delta L$ , overall lift of a quasi-elliptic wing.
$\ell$ , section lift.
$\Delta\ell$ , section lift given by a quasi-elliptic wing.
$n$ , number of quasi-elliptic wings; normal component of airloading.
$q$ , torque.
$r$ , radial location.
$R$ , rotor radius.
$\vec{s}$ , spanwise unit vector.

$t$ , tangential component of airloading.
$\vec{U}$ , inflow velocity.
$V$ , advancing speed along the rotor shaft.
$\vec{v}$ , induced velocity.
$v_n$ , normal component of induced velocity to rotational plane.
$v_t$ , tangential component of induced velocity to rotational plane.
$v_0$ , induced velocity on the rotational plane.
$v_1$ , induced velocity above the rotational plane.
$v_p$ , induced velocity component perpendicular to the local airflow.
$\Delta v_p$, perpendicular component of the induced velocity to the local airflow caused by each imaginary wing.
$v_q$ , induced velocity component parallel to the local airflow.
$\Delta v_q$, parallel component of induced velocity to the local airflow caused by each imaginary wing.
$\alpha$ , effective angle of attack.
$\Gamma$ , circulation.
$\Delta\Gamma$ , circulation of a quasi-elliptic wing.
$\lambda$ , inflow ratio, $\lambda = (V \sin i + v)/R\Omega$
$\theta$ , pitch angle.
$\rho$ , air density.
$\phi$ , inflow angle to the rotational plane, $\phi = \tan^{-1}(\frac{V}{r\Omega})$.
$\Phi$ , flow inclination angle, $\Phi = \tan^{-1}\{(V + v_n)/(r\Omega - v_t)\}$.
$\Omega$ , angular velocity.

subscripts

1 , inner edge of quasi-elliptic wing.
2 , outer edge of quasi-elliptic wing.
i , quantity of i-th quasi-elliptic wing.
k , quantity of k-th section.
m , mid point of quasi-elliptic wing.

## 1. INTRODUCTION

A rotary wing presents complicated aerodynamic phenomena in the flow field around the rotor. The complexity sometimes makes analysis employing a physically sophisticated model impractical or enormously time-consuming. The local momentum theory (LMT) was proposed as a practically useful method for calculating helicopter rotor aerodynamics. There are, however, some difficulties in applying this theory to rotary wings under various operating conditions, specifically under conditions of high axial flow field as encountered in windmills and propellers. In this paper, the differences between the operating conditions of a helicopter rotor and those of other rotary wings are discussed first. Then the fundamental equations of the LMT will be modified to those of an advanced computational method we call the "Local Circulation Method" (LCM) by which the airloading on a rotor blade operating in highly twisted flow can be calculated without wasting computation time.

## 2. LOCAL CIRCULATION METHOD

Shown in Fig. 1 is a rotor blade operating in axial flow, in which the inflow angle to the rotational plane, $\phi = \tan^{-1}(\frac{V}{r\Omega})$, varies appreciably along the span r/R for a high advance ratio $V/R\Omega$ and maintains a small value for a low advance ratio as shown in Fig. 2.

In the case of a helicopter rotor, the advance ratio $V/R\Omega$ or the inflow ratio $\lambda$ is on the order of $10^{-2}$, and the inflow angle $\phi$ changes greatly in the vicinity of the rotating axis but remains almost constant for any other station, i.e. $r/R > 0.1$. Since the rotor blade of a helicopter usually has a cut-off at the root, this drastic change near the axis does not have a significant influence on the calculation of airloading and thus the blade can be considered as operating in a uni-directional or flat flow field.

Unlike a helicopter rotor, a propeller or windmill works under large value of advance ratio $V/R\Omega$ and, therefore, a considerable change in the inflow angle occurs at every point on the blade. Thus the consequent flow around the blade and the trailing vortex sheet are highly twisted.

Fig. 3 illustrates the flow profile at an arbitrary section. Trailing vortex filaments do not lie on a flat plane. Induced velocities at the section caused by the respective vortex filaments consequently do not point in the same direction either. Thus the equation for local momentum balance adopted in the LMT can no longer be applied.

In the present method, the Kutta-Joukowsky theorem is applied to calculate the lift distribution without clarifying the relation between the induced velocity and the airloading. That is to say, by assuming the induced velocity to be small in comparison with the inflow velocity or $v \ll U$, the airloading can be related to the circulation distribution $\Gamma$ and to the elemental lift $\ell$ based on the blade element theory as follows:

$$\ell = \rho|\vec{U} + \vec{v}|\Gamma \simeq \rho U \Gamma \tag{1}$$

$$\ell \simeq \frac{1}{2}\rho U^2 ca(\theta - \phi - \frac{v_p}{U}) \tag{2}$$

where U is the absolute value of inflow velocity which is nearly equal to the total inflow velocity or $U \simeq |\vec{U} + \vec{v}|$.

The bound vortex $\Gamma$ and the perpendicular component with respect to the inflow velocity $\vec{U}$ of the induced velocity $\vec{v}$, $v_p$ are expressed in the form of summation given by those for n imaginary wings arranged one-sidedly in diminishing size as shown in Fig. 4,

$$\Gamma(r) = \sum_{i=1}^{n} \Delta\Gamma_i(r) \tag{3}$$

$$v_p(r) = \sum_{i=1}^{n} \Delta v_{p,i}(r). \tag{4}$$

That is to say, each pair of $\Delta\Gamma_i(r)$ and $\Delta v_{p,i}(r)$ corresponds to those of the i-th imaginary wing located in the same flow field, and satisfies the integration of the Biot-Savart law given by

$$\Delta\vec{v}_i = \frac{1}{4\pi}\int \frac{\vec{s} \times \vec{e}(r')}{r - r'} \frac{d\Delta\Gamma_i(r')}{dr'} dr' \qquad (5)$$

where $\vec{s}$ and $\vec{e}$ denote the spanwise and flowwise unit vectors respectively.

As the imaginary wing, a wing having an elliptical bound vortex distribution may be chosen. This is different from an elliptic wing, which is usually considered to have a constant induced velocity distribution on the wing surface in a flat flow field. Thus, the present imaginary wing having circulation distribution and operating in a twisted flow will hereafter be called a "quasi-elliptic wing."

Shown in Fig. 5 is a series of quasi-elliptic wings represented by the inflow velocity, and the circulation and induced velocity distributions. If the induced velocity outside the imaginary wings is neglected, the induced velocity and the bound vortex of k-th section can be related to each other from the first k quasi-elliptic wings,

$$\frac{1}{2}\rho U_k^2 c_k a \left(\theta_k - \phi_k - \frac{1}{U_k}\sum_{i=1}^{k}\Delta v_{p,ik}\right)$$

$$= \rho U_k \sum_{i=1}^{k}\Delta\Gamma_{ik} \qquad (6)$$

where $\Delta v_{p,ik} = \Delta v_{p,i}(r_k)$ and $\Delta\Gamma_{ik} = \Delta\Gamma_i(r_k)$.

The effect of neglecting the induced velocity outside the wing was discussed in Reference 1 for the case of flat flow field. The situation is unchanged in the present analysis. The calculation of the induced velocities caused by the respective quasi-elliptic wings is given in APPENDIX A.

Equation (6) and (A-5) determine aerodynamic variables of the k-th imaginary wing as follows:

$$\Delta\Gamma_k(r) = C_{\Gamma k}\sqrt{(r_{1k} - r)(r - r_{2k})} \qquad (7)$$

$$\Delta v_{p,k}(r) = A_k(r)C_{\Gamma k} \qquad (8)$$

and

$$C_{\Gamma k} = \left[U_k c_k a\left(\theta_k - \phi_k - \frac{1}{U_k}\sum_{i=1}^{k-1}\Delta v_{p,ik}\right)\right.$$

$$\left. - 2\sum_{i=1}^{k-1} C_{\Gamma i}\sqrt{(r_{1i} - r_k)(r_k - r_{2i})}\right]$$

$$/ \left[2\sqrt{(r_{1k} - r_k)(r_k - r_{2k})} + A_k(r_k)ac_k\right] \qquad (9)$$

where

$$A_k(r) = \frac{1}{4} - \frac{1}{2\pi}\sum_{i=1}^{n-k+2} \frac{\sin^2\{\frac{\phi(r_i') - \phi(r)}{2}\}}{r - r_i'} (H_{i+1} - H_i) \tag{10}$$

Equations (7) through (10) give the circulations (or lifts) and the perpendicular component of the induced velocities from the first section to the n-th section successively without iteration. Since, by assuming an inviscid fluid, the local lift is considered to be perpendicular to the total airflow which includes the induced velocity, the component of induced velocity parallel to the airflow can be directly calculated as follows:

$$\begin{aligned} v_{q,k}(r) &= \sum_{i=1}^{k} \Delta v_{q,ik}(r) \\ &= \sum_{i=1}^{k} \Delta v_{p,ik} \cdot \tan\{\phi(r_i') - \phi(r)\} \end{aligned} \tag{11}$$

$$\Delta v_{q,ik}(r) = -\frac{C_{\Gamma i}}{4\pi}\sum_{i=1}^{n-k+2} \frac{\sin\{\phi(r_i') - \phi(r)\}}{r - r_i'} (H_{i+1} - H_i) \qquad (r_{1k} \leq r \leq r_{2k}). \tag{12}$$

These two components, $v_p$ and $v_q$, are rewritten in other components for convenience; one in rotational plane, tangential induced velocity $v_t$, and the other normal to it, normal induced velocity $v_n$.

$$\left.\begin{aligned} v_t(r) &= v_p(r)\sin\{\phi(r) + \frac{v_p(r)}{U(r)}\} + v_q(r)\cos\{\phi(r) + \frac{v_p(r)}{U(r)}\} \\ v_n(r) &= v_p(r)\cos\{\phi(r) + \frac{v_p(r)}{U(r)}\} - v_q(r)\sin\{\phi(r) + \frac{v_p(r)}{U(r)}\}. \end{aligned}\right\} \tag{13}$$

Profile drag is calculated by employing experimental data and its direction is defined by including induced velocity. Then the forces working in the rotational plane, t, and normal to it, n, are finally given as follows:

$$\left.\begin{aligned} t &= \rho U\Gamma\sin(\phi + \frac{v_p}{U}) + \frac{1}{2}\rho U^2 c C_d \cos(\phi + \frac{v_p}{U}) \\ n &= \rho U\Gamma\cos(\phi + \frac{v_p}{U}) - \frac{1}{2}\rho U^2 c C_d \sin(\phi + \frac{v_p}{U}). \end{aligned}\right\} \tag{14}$$

The forces, t and n, and the induced velocity components, $v_t$ and $v_n$, determine a complete section aerodynamic state except for the torsional moment, which can be calculated easily if needed.

## 3. ATTENUATION COEFFICIENT

In order to take the induced velocity due to preceding wings into account, an attenuation coefficient is introduced just as in the LMT.[1)]

This coefficient represents the decay of induced velocity at any local station. Let us suppose a rotary wing which gives rise to an induced velocity or momentum change at the very moment it passes a space of interest. This induced velocity is taken as the effect of a preceding wing with respect to the succeeding wing and decreases in value as time ellapses by the attenuation coefficient C. Thus, the following wing is considered to go through the induced velocity field Cv.

The attenuation coefficient can be calculated by assuming a simple wake model. Shown in Fig. 6 are rigid wake models for a rotor in yawed flow. Only the tip vortices flowing with a constant speed are taken into account in these models. For the purpose of simplicity, the spiral wake model, (a), is split into a series of vortex rings and a series of axial vortex lines, (b), each laid on a wake cylinder.[2] When blades are rotating at low angular velocity or under high advance ratio, tip vortices make a thin spiral and airflow angles $\Phi$ and $\phi$ become large. These cause the induced velocity component in the rotational plane, which is mainly caused by axial vortex lines, to make a considerable change in airflow angle. However, in the present analysis, by assuming the tip speed of the rotary wing to be large enough, this effect of induced velocity in the rotational plane can be neglected. That is, the effect of the axial line model both on the normal component and on the in-plane component of induced velocity and the effect of the vortex ring model on the in-plane component are neglected. In physical terms, this means that the in-plane component of induced velocity vanishes immediately after the blade hits the space. The above simplification is not essential in the present analysis. It is, however, possible to introduce these effects into the calculation if required.

For practical calculation, the wake model given in Ref. 2 is employed and the attenuation coefficient is defined by the ratio of induced velocities $v_1/v_0$, where $v_0$ is evaluated at any station on the top of the cylinder and $v_1$ at the same station above the cylinder by the distance Z from the rotational plane which travels during the time of rotation $2\pi/b\Omega$ at the speed of inflow on the rotational plane.

Fig. 7 shows the calculated value of the attenuation coefficient. Since the wake model takes only the tip vortex into account, and the tip vortices are assumed to have an infinitesimal core, the singularity of $v_0$ on the edge of the rotational plane makes the coefficient zero at the tip.

In the calculation of inflow ratio, the simple momentum consideration can be applied as follows:

$$\lambda = \frac{V}{R\Omega}\sin i + C_T/2\sqrt{\left(\frac{V\cos i}{R\Omega}\right)^2 + \lambda^2} \qquad (15)$$

where i is the angle made by wind speed and blade rotational plane. In the case of axial flow or i = 90 degrees, equation (15) becomes a quadratic equation and $\lambda$ is given by

$$\lambda = \frac{1}{2}\left\{\frac{V}{R\Omega} + \sqrt{\left(\frac{V}{R\Omega}\right)^2 + 2C_T}\right\}. \qquad (16)$$

## 4. RELATIONSHIP BETWEEN THE LCM AND THE LMT

The LMT was developed to calculate the induced velocity and airloading distributions on the rotor blade of a helicopter rotor operating in hovering and advancing flight. It is based on the instantaneous momentum balance in combination with the blade element theory and the momentum theory. The momentum thoery gives the overall value of lift for each imaginary wing operating in an untwisted or flat flow field.

In highly twisted flow, however, only the circulation can simply be related to the elementary lift of the blade because, unlike the momentum vector, the circulation is a scalar, and the induced velocity on the lifting line cannot be related to the change in the momentum vector between the far upstream and far downstream portions of the wake. In the present method, the blade element theory is directly combined with the vortex theory as seen in equation (6), so this method has been called the "Local Circulation Method" and falls within the concept of vortex theory rather than momentum theory.

Fig. 8 shows the difference between the LMT and the LCM in the summations of lifts and induced velocities at an arbitrary section. In the LMT, all induced velocities point in one direction and the lift corresponding to each imaginary wing, $\Delta\ell_i$, is directed in the direction opposite that of the induced velocity. Therefore the lifts can be summed up in one direction which is the same as that of the actual lift. In the LCM, on the other hand, the lifts corresponding to the respective quasi-elliptic wings do not necessarily point in the opposite direction to the corresponding induced velocities. Therefore, the lift is calculated in relation to the intensity of the bound vortex which can be summed up as a scalar.

In order to show that the LMT can be derived from the LCM in the special case where the inflow ratio is small, it is sufficient to show that the local lift on any given quasi-elliptic wing can be predicted in terms of the momentum change on the lifting line and that the summation of these lifts at any section is equal to the lift actually acting there.

Assuming a small inflow ratio, the twist of flow field or the flow inclination angle $\Phi$ can be neglected and the inflow angle $\phi$ can, thus, be considered to be independent of the spanwise location. Since the effect of twist in the calculation for the respective quasi-elliptic wings in the APPENDIX A is reduced to zero, equation (8) can be expressed simply by equation (A-6) or

$$\Delta v_p = \frac{C_\Gamma}{4} \tag{17}$$

where the direction of $\Delta v_p$ is, in flat flow field, independent of the spanwise location and is normal to the rotational plane.

The air speed is given in a linear form,

$$U(r) = U_m + \frac{U_2 - U_1}{r_2 - r_1}(r - r_m) \tag{18}$$

where $U_m = (U_1 + U_2)/2$ and $r_m = (r_1 + r_2)/2$.

Then the lift distribution given by the Kutta-Joukowsky theorem is

$$\left.\begin{aligned}\Delta\ell(r) &= \rho U(r)\Delta\Gamma(r)\\ &= \rho C_\Gamma\{U_m + \frac{U_2 - U_1}{r_2 - r_1}(r - r_m)\}\sqrt{(r_2 - r)(r - r_1)}\\ &= 4\rho\Delta v_p\{U_m + \frac{U_2 - U_1}{r_2 - r_1}(r - r_m)\}\sqrt{(r_2 - r)(r - r_1)}.\end{aligned}\right\} \tag{19}$$

The last expression indicates that the local lift is related to the induced velocity or momentum change on the lifting line in the above simple case.

Let us consider the overall lift of an elliptic wing. Integrating equation (19) along the span of such a wing, the lift of the wing is given by

$$\begin{aligned}\Delta L &= \int_{r_1}^{r_2} \Delta\ell(r)\,dr\\ &= -2\{\rho\pi(\frac{r_2 - r_1}{2})^2 \frac{U_1 + U_2}{2}\}\Delta v_p.\end{aligned} \tag{20}$$

By eliminating $v_p$ from equations (19) and (20), section lift becomes

$$\Delta\ell(r) = \frac{4\Delta L}{\pi(r_2 - r_1)} \frac{U_m + \frac{U_2 - U_1}{r_2 - r_1} r}{U_m} \sqrt{(\frac{2}{r_2 - r_1})^2 (r_2 - r)(r - r_1)} \tag{21}$$

This equation is exactly the same as the expression for lift distribution given in the LMT except that it was originally given in non-dimensional form in Ref. 1.

Since the local lift is given in vectorial form as

$$\vec{\ell}(r) = \rho\Gamma(r)\vec{U} \times \vec{s} \tag{22}$$

where $\vec{s}$ denotes the spanwise unit vector, when the circulation $\Gamma(r)$ is given in summation form, the lift can be expressed by

$$\vec{\ell}(r) = \sum_{i=1}^{n} \{\rho\Delta\Gamma_i(r)\vec{U}(r) \times \vec{s}\}. \tag{23}$$

Each term of the right hand side of equation (23) obviously corresponds to the lift by an elliptic wing.

When the flow field is flat and the directions of all the terms of the summation in equation (23) are the same, equation (23) yields

$$\ell(r) = \sum_{i=1}^{n} \Delta\ell_i(r) \tag{24}$$

$$\Delta\ell_i(r) = \rho U(r)\Delta\Gamma_i(r). \tag{25}$$

Since the respective lifts of equation (25) are written in terms of induced velocity $v_p$ as shown in equation (19), the above relations demonstrate the previous statement and show the linearity of lift in the LMT and in the case of low inflow ratio in the LCM.

The section drag is similarly given by

$$d = \sum_{i=1}^{n} \frac{1}{2} \rho U^2(r)c(r)C_d(r). \tag{26}$$

## 5. STALL CONSIDERATION

It is seen in Fig. 2 that the inflow angle varies along the span for a high advance ratio and that the rate of twist of flow field is dependent on the inflow ratio under which the rotary wing is operating. This variation in the twist of the airflow with the value of the inflow ratio can not always be compensated for by wash-out in a propeller or wash-in a windmill. In addition, in the case of windmills, the wind speed and direction cannot be controlled and it is difficult to maintain operation under near optimal conditions. Thus, an analysis of a rotary wing operating under stall condition becomes indispensable.

In the present analysis, the vortex theory is assumed to be still applicable under stall condition. Therefore, the amendment required in the present method should be performed in its usage of the blade element theory. To include the stall effect, equation (6) and (9) should be modified as

$$\frac{1}{2} \rho U_k{}^2 c_k C_\ell(\alpha_k) = \rho U_k \sum_{i=1}^{k} \Delta\Gamma_{ik} \tag{27}$$

and

$$U_k c_k C_\ell(\alpha_k) = 2\sum_{i=1}^{k-1} C_{\Gamma i}\sqrt{(r_{1i} - r_k)(r_k - r_{2i})} + 2C_{\Gamma k}\sqrt{(r_{1k} - r_k)(r_k - r_{2k})} \tag{28}$$

where the circulation of the blade element has been represented by that given at mid point of that section instead of the mean value and where $\alpha_k$ is the effective angle of attack,

$$\alpha_k = \theta_k - \phi_k - \frac{1}{U_k}\sum_{i=1}^{k-1} v_{p,ik} - \frac{1}{U_k} A_k(r_k)C_{\Gamma k}. \tag{29}$$

Equation (28) cannot be solved analytically now due to the complexity of lift coefficient $C_\ell(\alpha_k)$. Attention should also be paid to the numerical value of drag coefficient $C_d$ in using equation (14), and (26).

Knowing the lift and the drag distribution, the section torque of a windmill is given by

$$q = \ell \sin \Phi - d \cos \Phi. \qquad (30)$$

A typical example of the angle of attack, normal force and torque distributions of a windmill is seen in Fig. 9. This rather flat distribution is mainly caused by giving a taper distribution to the blade. A fair change in the lift inclination and a rather small change in airspeed along the span due to the large value of advance ratio also contribute to the flatness of this distribution.

If, however, a stall once occurs at some point on the blade, this distribution changes appreciably. Usually, both the change of flow inclination angle corresponding to the change of advance ratio or inflow ratio at the blade root and the contribution of the blade root to overall torque are so large in windmills that the stall effect is severe for such a flat torque distribution. It should be noted that when a blade is operating under stall condition and the value of the flow inclination angle $\Phi$ is low there, both terms on the right hand side of equation (30) can be of the same order and the windmill rotates in a subtle balance of airloading. More precise estimation of the lift and drag coefficients will be necessary for the calculation of windmill airloading under such operation.

## 6. NUMERICAL EXAMPLES

In order to verify the validity of the present method, a calculation of the propeller performance was carried out, and the results were compared with the theoretical results obtained by other methods and with experimental results. In this calculation, the attenuation coefficient was assumed to be independent of the location in the rotational plane, and equal to that of the calculated value at three-quarter-radius point. The performances of the propellers in Ref. 4 were predicted.

Table 1 and Fig. 10 a) and b) give the specifications of the propellers. The aerodynamic coefficients for a two-dimensional airfoil used in this calculation were estimated by referring to the experimental data for the wing of aspect ratio 6 given in Ref. 5. These estimated values are presented in Fig. 11.

A comparison with the experimental data and with the results of other methods is shown in Fig. 12 to 15. The results by the present method are in generally good agreement with the experimental results. A small discrepancy appears when the geometric pitch angle is large and the advance ratio is small. This is no doubt caused by the rather low lift slope and the fact that the effect of the thickness ratio and the Reynolds number on the maximum lift coefficient were disregarded.

The LCM, like the LMT, is characterized by its ability to permit rapid and approximate calculation of the distribution and the fluctuation of airloading and induced velocity in non-axial flow rather than by its ability to provide exact solutions.

The time variations of bending moment at the blade root, local and overall thrusts, and airloading and induced velocity distributions for the propeller in yawed flight are presented in Figs. 16 to 18. The blade is assumed to rotate clockwise as seen from downstream and the azimuth angle is measured from the downstream. The attenuation coefficient is assumed constant over the rotational plane and is evaluated at the radius of 0.75R and the azimuth angle of 90 or 270 degrees. Since the trailing vortices flow at high advance ratio, the effect of crossing a tip vortex is not remarkable.

The most prominent effect appears near the blade tip and at an azimuth angle of 120 degrees where the blade travels at so high speed that it comes across the vortex core before it flows away. In Fig. 18 (a) and (b) the perspectives of airloading and induced velocity are given for the azimuth angles of 90 and 270 degrees. It is seen in these figures also that the clear effect of the preceding blade tip vortex appears near 80% span of advancing side blade as shown by arrow symbols and that the effect is not clear in the retreating side blade.

## CONCLUSION

The local momentum theory was extended for highly twisted flow by relying on the vortex theory and was made applicable to rotors operating in high axial airspeed. This method of calculation makes it possible to analyze the dynamic airloading and induced velocity distribution of propellers and windmills without requiring an enormous amount of computation. The comparison of the results with those of experimental and other theoretical methods showed that the present method gave a good prediction and that it was useful for the analysis of rotary wings under any operating conditions. The present method is also applicable to the rotary wing in yawed flight. An example of the calculation for a propeller in yawed flight was also presented.

## APPENDIX A. CALCULATION OF INDUCED VELOCITY DUE TO AN ELLIPTIC WING IN TWISTED FLOW FIELD

Calculation of the perpendicular component of induced velocity to the airflow at the section of interest, $v_p$, is treated here. Let us consider a bound vortex distributed in section partitioned off by two spanwise stations $[r_1, r_2]$. The trailing vortex is assumed to flow straight backward in the direction of airflow at the section, i.e. in the direction $\vec{U}$.

The perpendicular component of induced velocity at an arbitrary section r is given by

$$\Delta v_p(r) = \frac{1}{4\pi}\int_{r_1}^{r_2} \frac{\cos\{\phi(r') - \phi(r)\}}{r - r'} \frac{d\Delta\Gamma(r')}{dr'}\, dr'. \qquad \text{(A-1)}$$

Equation (A-1) is modified as

$$\Delta v_p(r) = \frac{1}{4\pi}\int_{r_1}^{r_2} \frac{1}{r - r'} \frac{d\Delta\Gamma(r')}{dr'} dr'$$

$$- \frac{1}{2\pi}\int_{r_1}^{r_2} \frac{\sin^2\{\frac{\phi(r') - \phi(r)}{2}\}}{r - r'} \frac{d\Delta\Gamma(r')}{dr'} dr'. \quad \text{(A-2)}$$

Thus the singularity can be attributed to the first integration only, provided that $\phi = \phi(r')$ is differentiable. The second integration is considered to be the effect of twist. A non-twisted flow, $\phi$ = constant, makes it zero and does not affect the first integration. Furthermore, if the bound vortex $\Delta\Gamma$ is distributed elliptically in $[r_1, r_2]$ and the section of interest falls between $r_1$ and $r_2$, then the first integration results in a constant,

$$\Delta\Gamma(r) = C_\Gamma\sqrt{(r_1 - r)(r - r_2)} \quad \text{(A-3)}$$

$$\Delta v_p(r) = \frac{C_\Gamma}{4} - \frac{1}{2\pi}\int_{r_1}^{r_2} \frac{\sin^2\{\frac{\phi(r') - \phi(r)}{2}\}}{r - r'} \frac{d\Delta\Gamma(r')}{dr'} dr'. \quad \text{(A-4)}$$

If the integration is replaced by summation as shown in Fig. A-1, the above equation yields

$$\Delta v_p(r) = \{\frac{1}{4} - \frac{1}{2\pi}\sum_{i=1}^{n+1} \frac{\sin^2\{\frac{\phi(r_i') - \phi(r)}{2}\}}{r - r_i'} (H_{i+1} - H_i)\}C_\Gamma$$

$$r_i' = r_i + \frac{r_2 - r_1}{n}(i - 1)$$

$$H_i = \begin{cases} 0 & i = 1 \text{ and } i = n + 2 \\ \frac{1}{\xi_i - \xi_{i-1}}(\xi_i\sqrt{1 - \xi_i^2} - \cos^{-1}\xi_i - \xi_{i-1}\sqrt{1 - \xi_{i-1}^2} + \cos^{-1}\xi_{i-1}) & 2 \le i \le n + 1 \end{cases} \quad \text{(A-5)}$$

$$\xi_i = \frac{2r_i' - (r_1 + r_2)}{r_2 - r_1}.$$

When a less time-consuming calculation is required, the second term of equation (A-4) can be neglected, reducing the equation to the following simple one.

$$\Delta v_p = \frac{C_\Gamma}{4}. \quad \text{(A-6)}$$

It should be noted that this equation does not imply a uniform induced velocity field because its direction is defined normal to the airflow, the direction of which changes along the span.

# REFERENCES


1. A. Azuma, K. Kawachi — Local Momentum Theory and its Application to the Rotary Wing. J. of Aircraft (1979) 16 (1) 6-14

2. W. Castles Jr., J. H. De Leeuw — The Normal Component of the Induced Velocity in the Vicinity of a Lifting Rotor and Some Examples of its Application. NACA Report 1184 (1954)

3. R. T. Griffiths — The Effect of Aerofoil Characteristics on Windmill Performance. Aeronautical J. (1977) 322-326

4. D. Biermann, E. P. Hartman — Tests of Two Full-Scale Propellers with Different Pitch Distributions at Blade Angles up to 60°. NACA Report 658 (1938)

5. D. H. Wood — Tests of Large Airfoils in the Propeller Research Tunnel Including Two with Corrugated Surface NACA Report 336 (1929)

Table 1. Dimensions of the rotor, common to propeller I and propeller II

| Items | | |
|---|---|---|
| Rotor radius , | R | 1.52 m |
| Number of blades , | b | 3 |
| Solidity , | σ | 0.0898 |
| Aerofoil section , | | Clark Y |
| Chord length , | c | refer to Fig. 10 |
| Thickness ratio , | t/c | refer to Fig. 10 |
| Pitch distribution, | θ | refer to Fig. 10 |

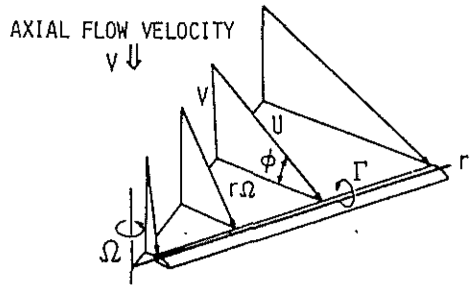


Figure 1. A rotating blade in axial flow.

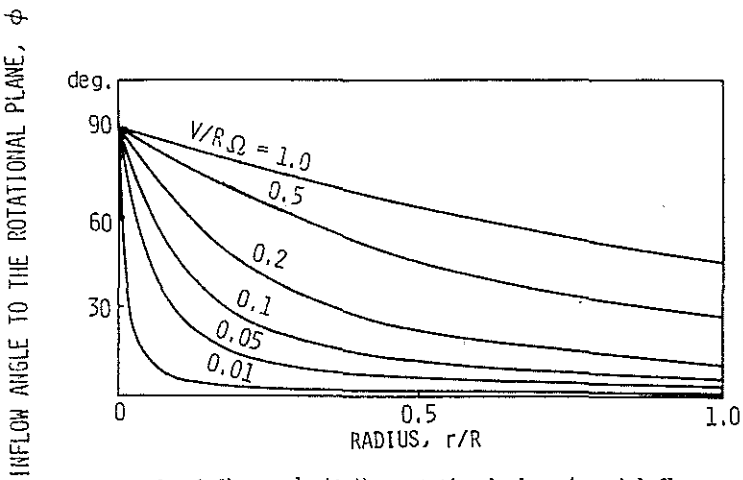


Figure 2. Inflow angle to the rotational plane in axial flow.

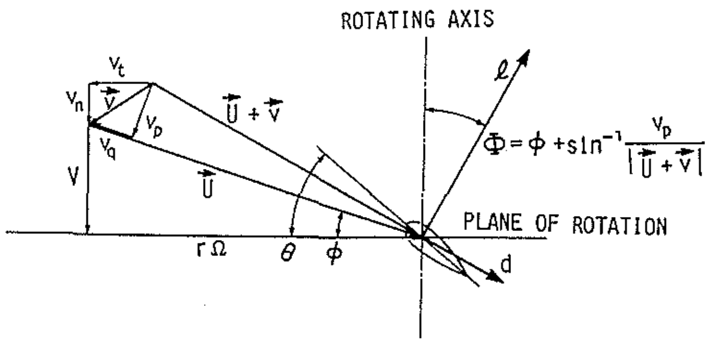


Figure 3. Airflow and force configuration.

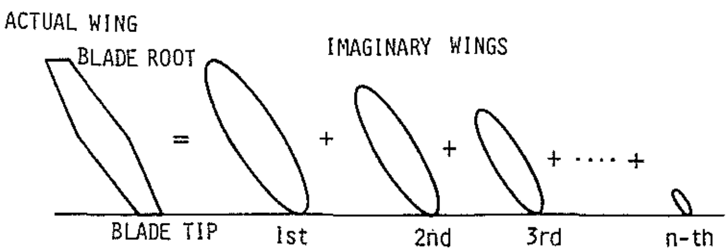


Figure 4. Decomposition of a wing into n imaginary wings.

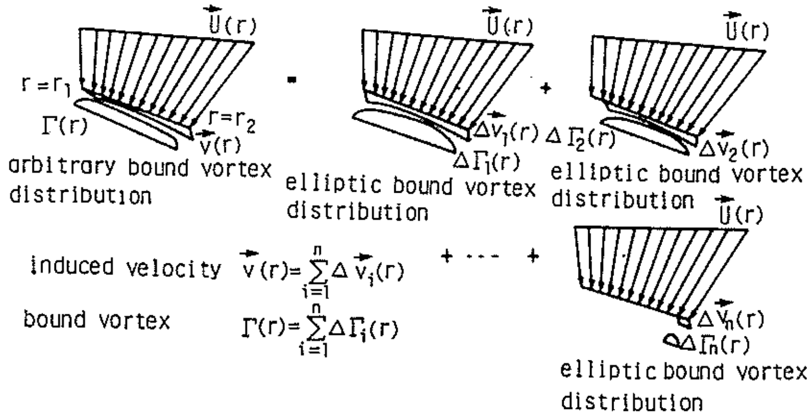


Figure 5. Superposition of quasi- elliptic wings.

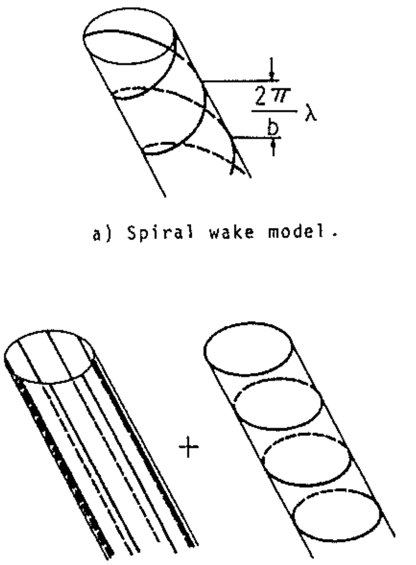


a) Spiral wake model.

b) Vortex rings and axial vortex lines on the wake cylinder.

Figure 6. Rigid wake models.

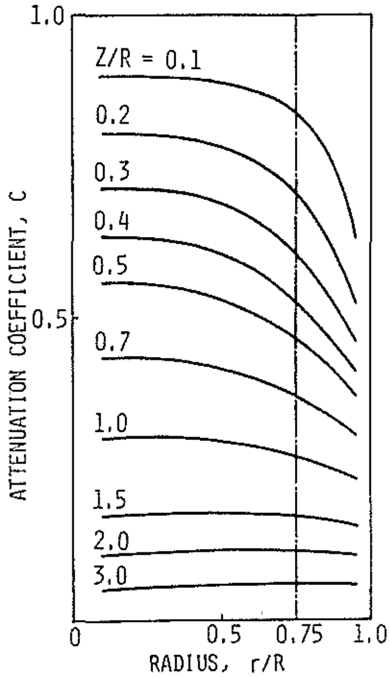


Figure 7. Attenuation coefficient.

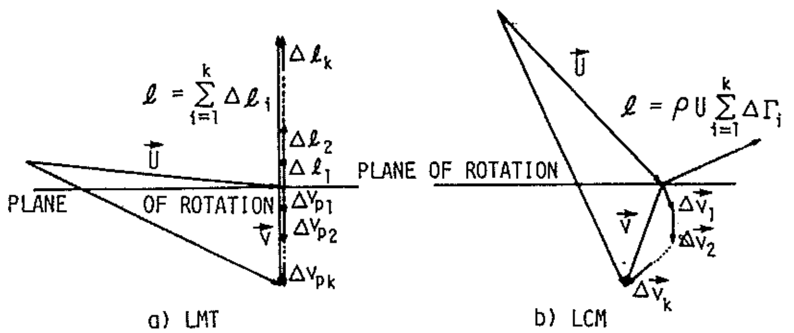


Figure 8. Summation of lifts and induced velocities in the LMT and in the LCM.

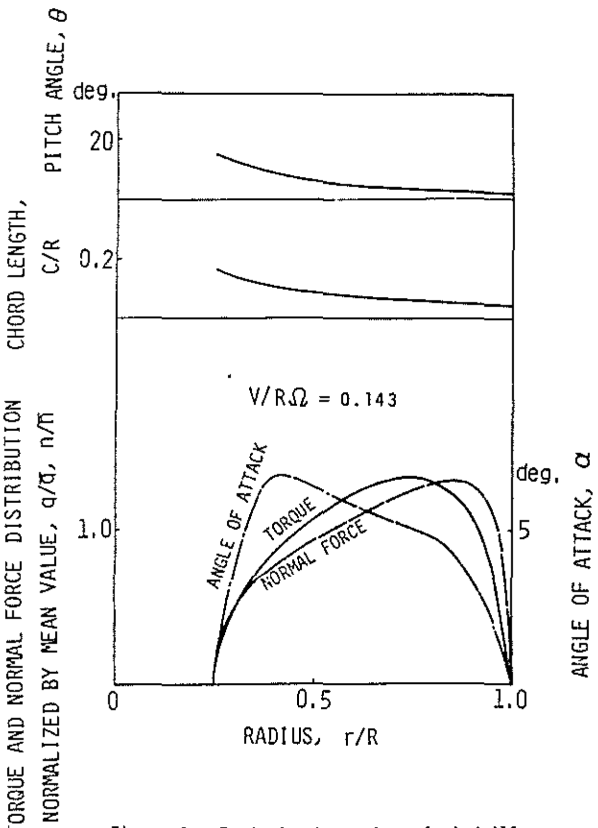


Figure 9. Typical airloading of windmill.

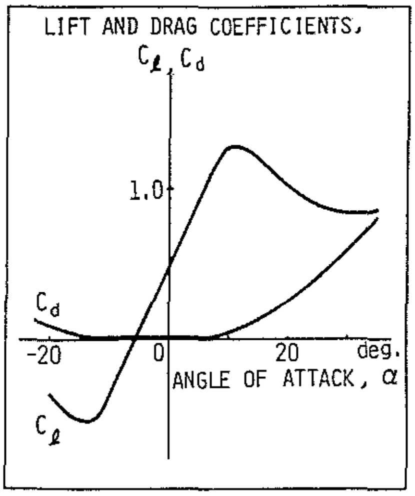


Figure 11. Lift and drag coefficients for Clark Y section airfoil, estimated from NACA Report 336.

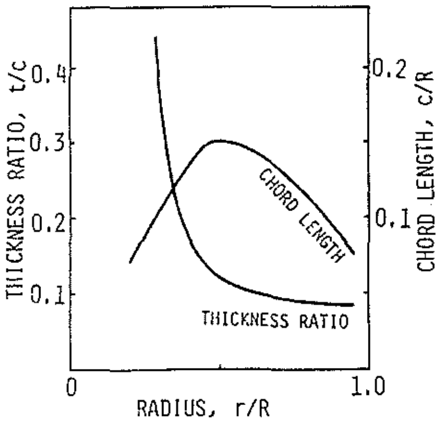


Figure 10 a). Planform of propeller.

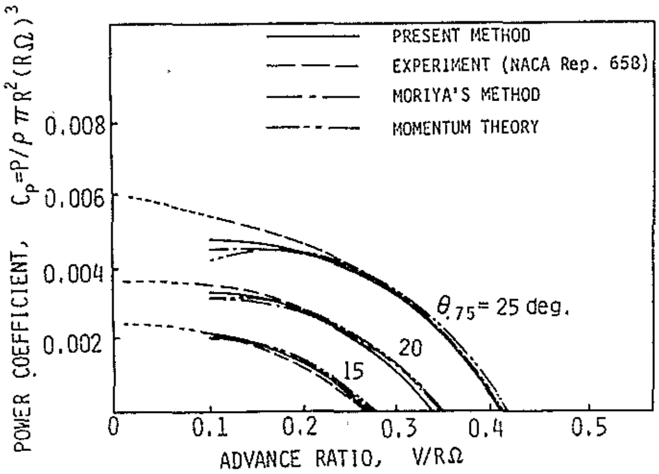


Figure 12. Power coefficient for propeller I.

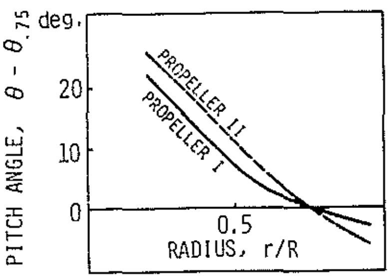


Figure 10 b). Pitch angle distribution.

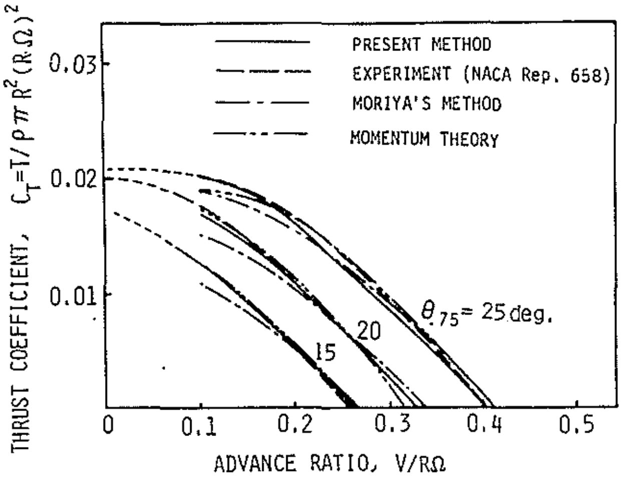


Figure 13. Thrust coefficient for propeller I.

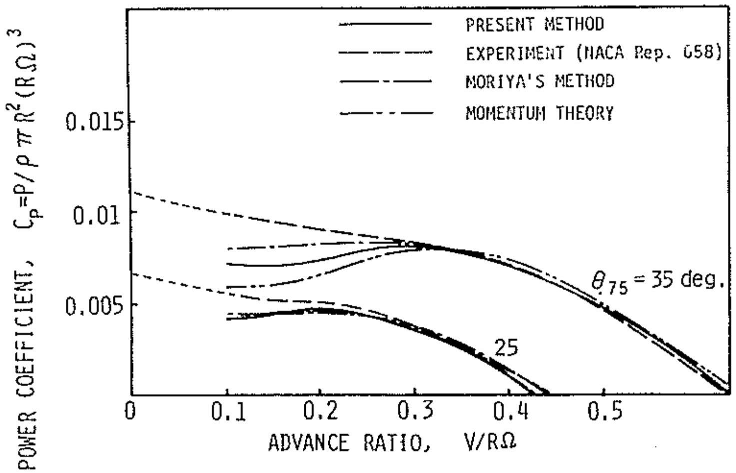


Figure 14. Power coefficient for propeller II.

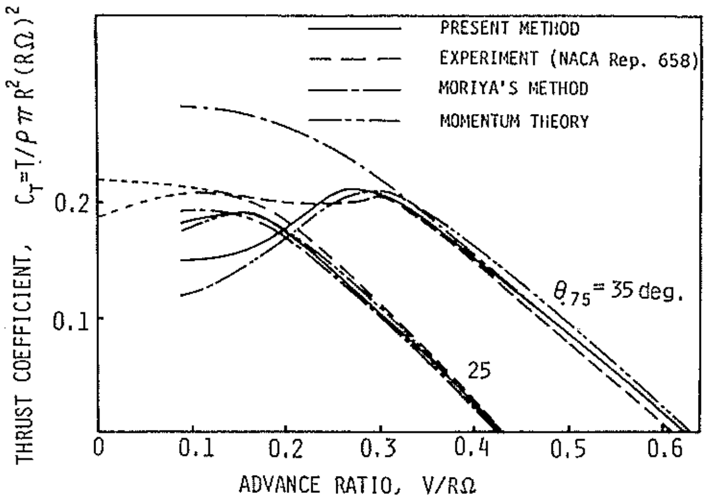


Figure 15. Thrust coefficient for propeller II.

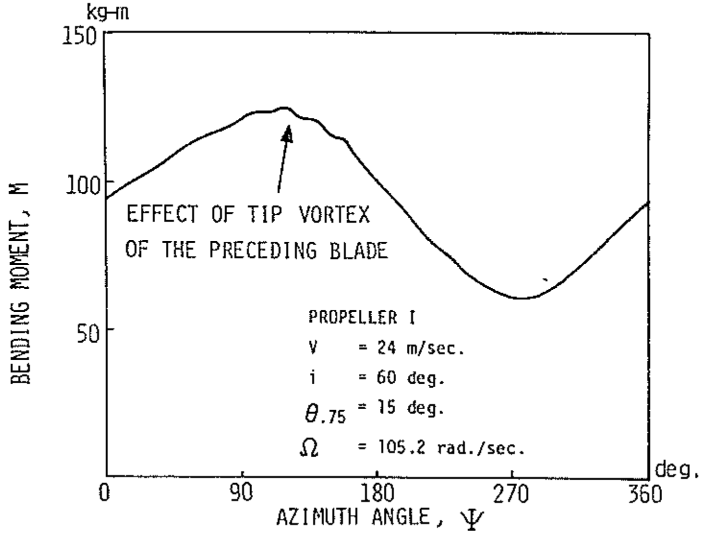


Figure 16. Blade bending moment.

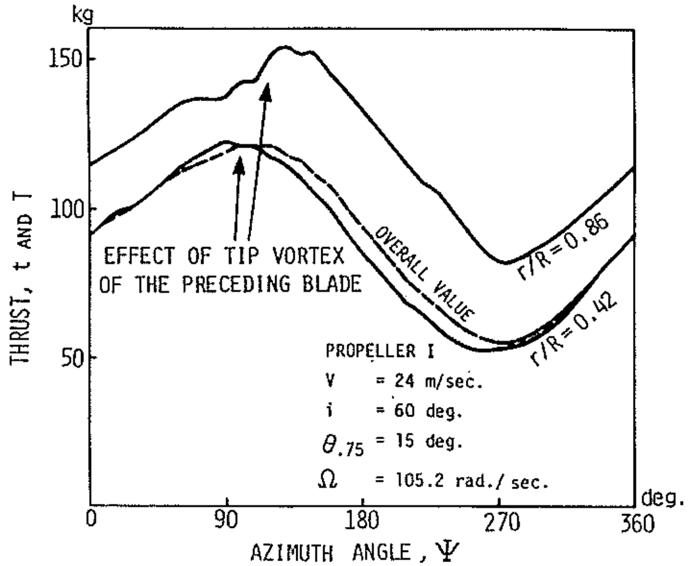


Figure 17. Local and overall thrust of a blade.

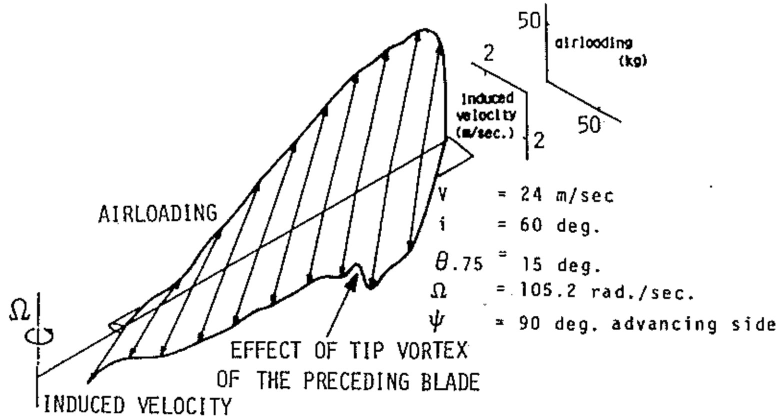


Figure 18 a). Perspective of airloading and induced velocity distribution.

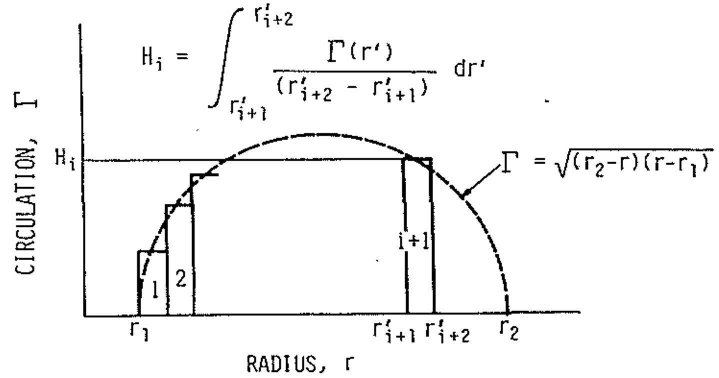


Figure A-1. Approximation of elliptically distributed bound vortex.

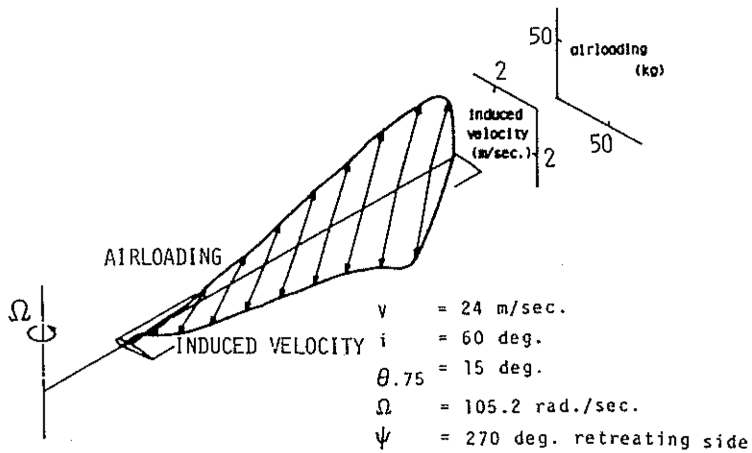


Figure 18 b). Perspective of airloading and induced velocity distribution.